



Creation of fine lath martensite combined with nano needle like structured carbides in ultra high strength (UHS) military Steel

Maha El-Meligy^{1*}, Taher El-Bitar¹, Saad Ebied²

¹Plastic Deformation Dept., Central Metallurgical R&D Institute (CMRDI), 1st Elfelazaat St., El-Tabeen, 11722 Helwan, Egypt;

²Department of Production Engineering and Mechanical Design, Faculty of Engineering, Tanta University, Tanta 31527, Egypt.

Received: 20 September 2023; Accepted: 14 December 2023

*Corresponding author email: dr.mahaemeligy@gmail.com

ABSTRACT

The steels of the current study contain 0.3% carbon with different amounts of Cr, and Mo, in addition to W. The steels were cast as Y-blocks. Cast slabs with 150x100x35 mm dimensions were then subjected to 4-steps directional hot forging into 15 mm diameter round bars in the temperature range 1200-830 °C. Austenite grain refinement was taken place by the 4-steps cross-sectional reductions, where it secures fine lath martensite combined with crammed nano needle-like $Cr_{23}W_2C_6$ carbides between the martensite laths. A quenching tempering cycle was carried on the forged bars at 250 °C for 25 min. and then air cooled to modify the martensite laths and reorganize the nano needle-like carbides to modify the mechanical properties. The optical microscopic investigation confirms extensive grain refining of the martensite laths. However, scanning electron microscope (SEM) photos at high magnifications reveal. The structure composed mainly of fine laths martensite with nano needle-like structured carbides with 50 nm diameter crammed between the martensite laths. Little amounts of retained austenite (RA) phase was located tightening on the boundaries of martensite laths as white nano films. A blend of -fine laths martensite and nano films of retained austenite (RA) phases in addition to the crammed nano needle-like structured carbides are working cooperatively for ultra-high strength creation. The tensile test specimens possessed continuous yielding, as the predominant microstructure contains a martensite phase. Strength increases continuously due to tungsten (W) addition up to 1.6%. During tempering, some of the nano needle-like $Cr_{23}W_2C_6$ carbides, which were crammed between the martensite laths have a chance to migrate out from the martensite laths. The migrated nano needle carbides favor to coagulate and stick to each other to form 3D nano bulk-size spheroidal shaped carbides sizing 200 nm and precipitating on the martensite laths surface.

Keywords: Ultra high strength (UHS) steel, Tungsten alloying, Multiple step forging, Martensite Laths, Crammed nano needle-like carbides, Quenching-tempering processing.

1. Introduction

Tungsten containing steel is designed to achieve both comparable strength and toughness by limiting the nickel and cobalt alloying elements and offset by a tungsten addition. Furthermore, tungsten (W) is a common substitute for molybdenum (Mo), because it has similar carbide formation behavior [1]. Tungsten forms persistent carbides of

the type $W_{23}C_6$ that possess a coherent interface, which would precipitate on the austenite grain boundaries. $W_{23}C_6$ carbides could be solution treated at 1050 – 1150 °C before hot forming [2].

The steel is primarily processed by forging and/or hot rolling. Hot deformation breaks up the as-cast dendritic structure and homogenize the matrix thereby reducing micro-segregation. Upon austen-

itizing, the carbide forming elements (W, Mo and Cr) are stable and distribute in the austenite matrix. A subsequent rapid quenching prevents the formation of large size carbides, where the carbide forming elements are trapped within the martensitic laths [1].

A detailed study for microstructure evaluation of a C-steel containing W, assured that carbide clusters start to form when quenched steels are heated to 100 °C or above, and these carbide clusters eventually grow to become ε-carbides [3].

Controlled processing in hot deformation is

usually used for martensitic structure uniformity and grain refinement [4]. Multiple-directional forging was used [4], in order to improve the microstructure uniformity of UHS martensitic steel at a strength higher than 2500 Mpa. Controlling of the deformation temperature, amount of strain in addition to the strain rate can be effectively used for refining the martensite matrix, which would improve the toughness [5] and reduce undesirable brittleness [6] of high strength steels. Repeated hot deformation of austenite grains by multiple-pass hot rolling would result in obtaining uniform and

Table 1- Chemical Composition of the steels

Element, wt.% Alloy	C	Si	Mn	P	S	Cr	Mo	Ni	Al	W
Pen St. 1	0.334	0.852	1.05	0.022	0.010	2.48	0.293	0.913	0.122	0.945
Pen St. 2	0.337	0.829	1.06	0.024	0.017	2.45	0.310	0.913	0.130	1.41
Pen St. 3	0.312	0.814	1.03	0.023	0.010	2.48	0.294	0.917	0.123	1.63
Pen St. 4	0.321	0.785	0.979	0.024	0.013	2.43	0.307	0.906	0.104	2.01

Table 2- Mean critical and allotropic transformation temperatures of the 4 steels

Critical and allotropic temperatures	Ac ₁	Ac ₃	M _s	M _f	B _s
Values in °C	774	796	276	100	442

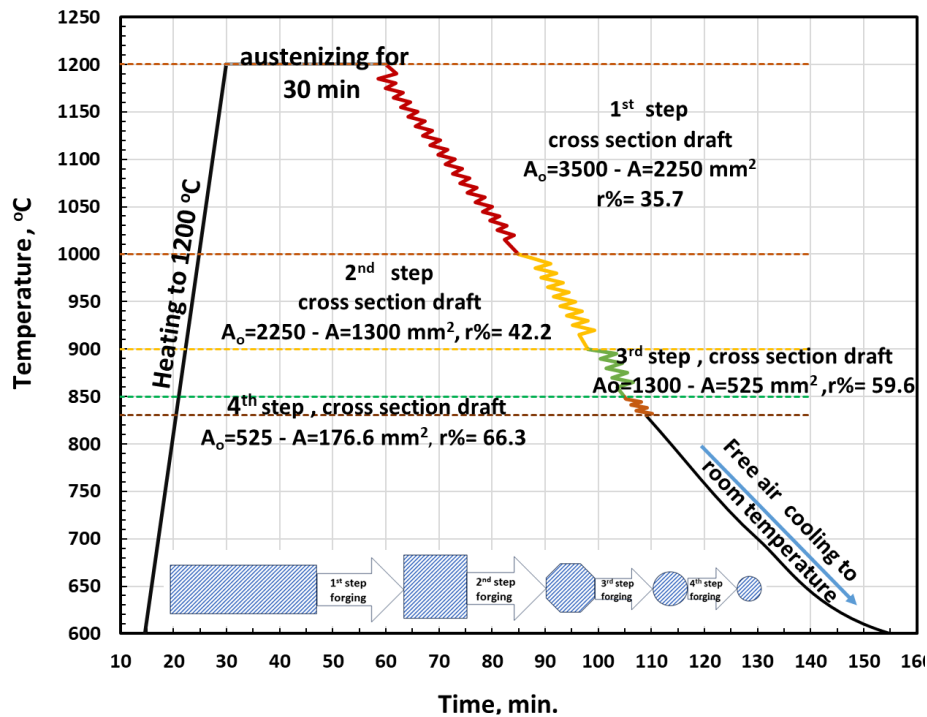


Fig. 1- Schematic presentation of the 4-step hot forging process.

fine through martensitic-bainitic structure [7].

Piercing capacity of penetrators would be further improved to confront the armor steel improvements. Consequently, kinetic energy penetrators should possess the best combination of hardness, stiffness, strength, and fracture toughness characteristics to be effective against modern armor systems. Over the last decade, depleted uranium (DU) and tungsten containing steels (WA) have been the materials of choice for kinetic energy penetrators. DU outperforms WA penetrators, but because of environmental concerns, efforts have been focused on improving the performance of WA penetrators over the last few years [8-10].

Martensitic transformation steels are rarely used in an untempered condition, where tempering increases both ductility and toughness, which are essential for enhancing dynamic impact energy absorption. On the other hand, $W_{23}C_6$ is precipitated during tempering, where softening of martensite is retarded preventing the loss of notch toughness resulting from these persistent alloy carbides [11]. Previous results showed that tempering at 200°C gives the best ballistic performance [12], while in some other work, 300 °C was favored for best ballistic properties of a high strength armor steel [5].

Lightly, tempered martensitic/bainitic microstructure of UHS containing steel produces good toughness and continuous yielding during tensile loading. A high degree of strain hardening is achieved, as indicated by a yield strength/tensile strength ratio (YS/TS) of 0.8. The more highly alloyed steels typically exhibit YS/TS ratios of 0.9.

High strain rate tensile testing has demonstrated good performance at impact-like strain rates [13].

The current work investigates how multiple steps directional hot controlled forging parameters are effectively used for creation of fine laths martensite phase combined with nano needle like structured carbides in ultra-high strength (UHS) Military Steel. Attention is also focused on the tempering process parameters and effects to modify the steel properties.

The current article is dealing the strengthening of W- bearing military steel, which is used for dynamic energy penetrators. The novelty in the present article was concluded as a blend of fine laths martensite and nano films of retained austenite (RA) phases in addition to the crammed nano needle-like structured carbides are working cooperatively for ultra-high strength creation.

2. Experimental Work

The steels were developed at the experimental foundry shop in CMRDI of Egypt. Table 1 presents chemical composition of steels under investigation. The steels were cast as Y-shape blocks with a sound ingot dimensions 300x200x35 mm [14].

The Critical and allotropic transformation temperatures were evaluated by using the commercial software package “J Mat pro” [14]. The mean critical and allotropic transformation temperatures are considered in Table 2, where variations in different temperatures between the 4 steels are ranging 5 °C max.

The sound parts of the cast ingots were then

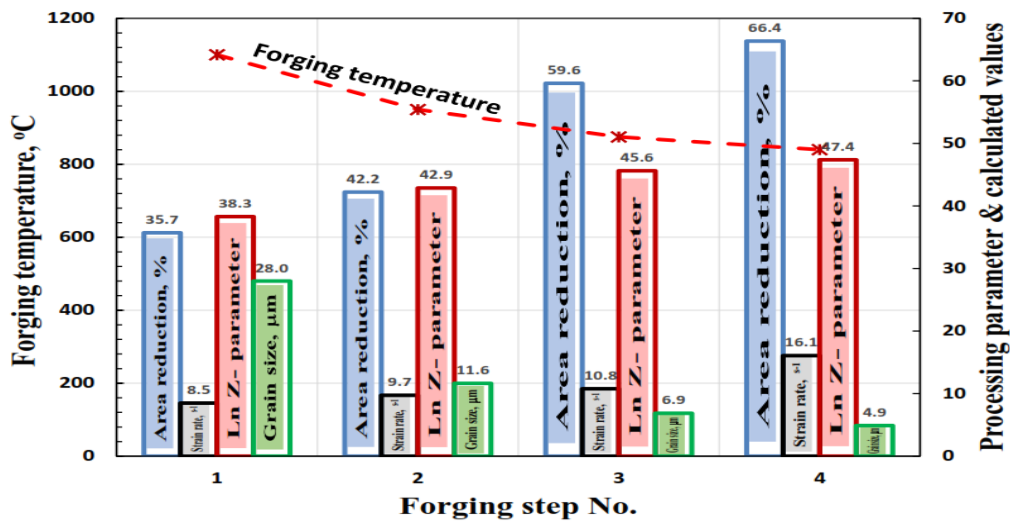


Fig. 2- Different process parameters and calculated values.

subjected to 4-steps directional hot-controlled forging into round bars with 15 mm diameter in the temperature range 1200-830 °C. Fig.1 presents schematically the 4-steps directional hot forging process

The 4-steps directional hot forging process was aiming at bilateral effects. The 1st one is the shape and dimensional changes, while the 2nd effect is the strength enhancement. The shape is changed from rectangular to square and followed by octagon then round rod and finally to round bar as presented in

Fig. 1.

During the forging process velocity was previously calculated as 300 mm/sec [6] and the activation energy (Q) for deformation was considered as 537 KJ/mole [15]. The grain size (D) after each deformation step can be expected as $D \text{ (um)} = 3.373 \times 10^3 Z^{-0.192}$ [16]. Fig.2 summarizes different process parameters and calculated values.

Suitable samples were then taken from the forged bars for X-ray diffraction analysis (XRD) and microstructure investigations. Tensile and

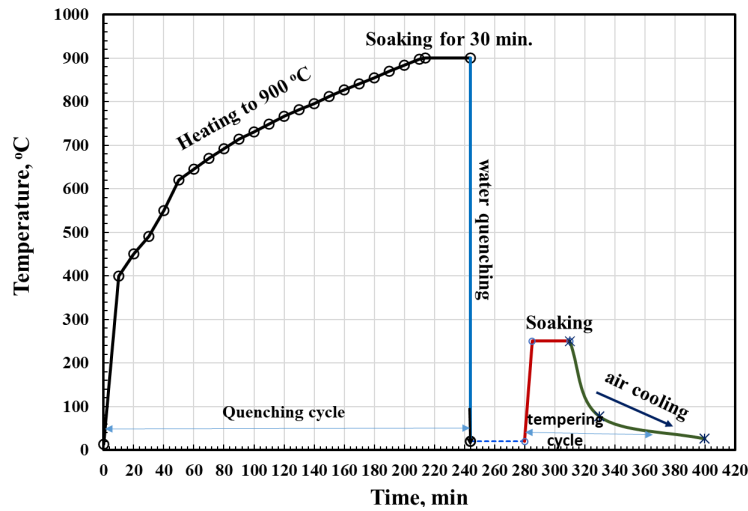


Fig. 3- Schematic presentation of water quenching and tempering cycles.

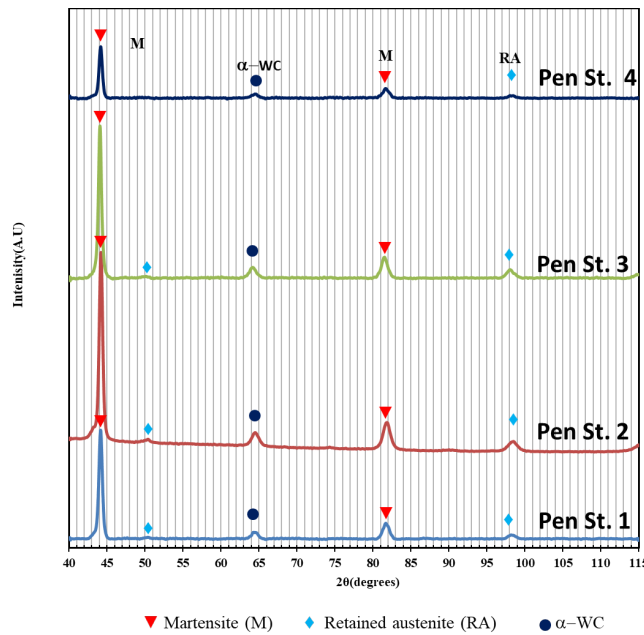


Fig. 4- XRD phases intensity charts of different steels.

hardness testing were also carried out for mechanical characterization of the forged bars. Fig.3 presents schematically the water quenching and tempering cycles, which were additionally carried out at 250 °C for 25 min.

3. Results and Discussions

XRD investigations were used for exploring the coexisting phases in the different steels. Fig. 4 presents phase intensity charts of the coexisting phases in 4-steps forged steels. The XRD charts ensure that the steels possess martensite (M) matrix containing a considerable amount of remnant tungsten carbides of the alloying elements (α -WC) and few amounts of retained austenite phase (RA). $M_{23}C_6$ is usually a Cr-rich carbide having the complex fcc structure of $Cr_{23}C_6$. However, elemental Tungsten (W) was observed to go into solution in the Cr-rich carbide lattice, forming $Cr_{21}W_2C_6$ [17]. On the other hand, it was concluded that an accumulation of RA in the steels would negatively affect ductility of the whole structure [11]. Furthermore, many of previous studies [11, 18, 19] insured that (RA) is usually created at inter lath and appear as a white film.

The previous by Fig. 2 clearly shows that the forging temperature decreases from a deformation step to the other, while both of the amount of reductions in cross section area and strain rates

increase continuously. Consequently, the numerical calculations ensure exaggerated increase of the Z-parameter, which would be reflected positively on the austenite grain size refinement. The expected grain size (D) is starting with 3.5 μm at the 1st deformation step, where the mean forging temperature was high as 1100 °C and the strain rate was low. On the other side, D becomes 0.6 μm on finishing at the 4th step with a lower temperature at 830 °C and higher strain rate. On cooling after the 4-steps of the deformation sequence, fine martensite laths structure is assured.

Fig. 5 presents optical microscopic photos for 4-steps cross sectional reduction forgings for steels Pen St.1 and Pen St.3. It is clear that microstructure of both steels reveal fine martensitic structure side by side with likely remnant alloying elements carbides (black points) and retained austenite segregation (white elongated regions). The white regions are created and arrayed parallel to the forging directions and located at the inter-martensite laths [11, 19].

Detailed microstructures, of deep etched-polished surfaces, were obtained by using the scanning electron microscope (SEM) at high magnifications for further clarification and better understanding. Fig. 6 presents the microstructure of different steels at a high magnification. All micrographs confirm what the optical microstructure showed in Fig. 5.

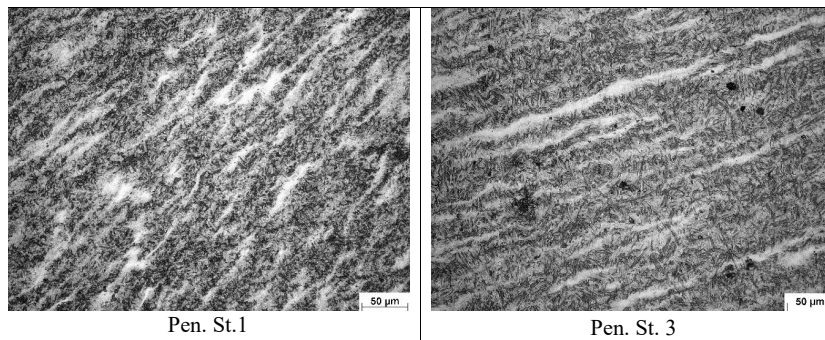


Fig. 5- Optical microscopic photos for 4-steps cross sectional reduction forgings of steels Pen St.1 and Pen St.3.

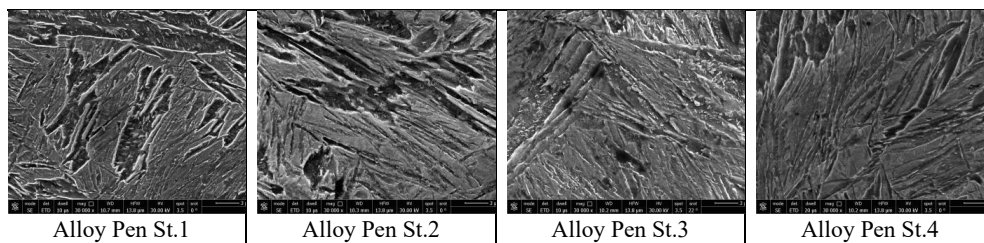


Fig. 6- SEM micrographs presenting ultra fine lath martensite structure.

High magnification microstructures presented in Fig. 6, are revealing fine martensite laths.

However, it is necessary to go for further higher magnifications to detect nature and distribution of the carbides and retained austenite. Fig. 7 presents more detailed constituents for steels Pen St.1 and Pen St.2 at a higher magnification. Nano needle-like structured carbides with 50 nm diameter are found crammed and located between the - fine martensite laths, which is confirmed with nature and location of the carbide precipitate in ref. [20].

In some other locations on the polished etched surface, Fig. 8 shows micrographs for steels Pen St.3 and Pen St.4 at a higher magnification. Clear nano films of retained austenite (RA) are tightening on the grain boundaries of the fine martensite laths [20].

A blend of fine martensite laths and nano films of retained austenite (RA) phases in addition to the crammed nano needle-like structured carbides are working cooperatively for ultra-high strength creation [21].

The tensile properties of the different steels are presented in Fig. 9 as Engineering stress - Engineering strain relationships. It is quite clear that strength is increased due to W-addition up to 1.6%, after which at 2.0% W, both strength and strain are decreased. Furthermore, the steels under investigation possess continuous yielding, where the predominant microstructure contains martensite phase [22], as previously investigated and presented by XRD phase intensity charts in Fig. 4 and optical microstructure in Fig. 5.

It can be expected that up to 1.6% tungsten may go into solution and accommodate in the carbide lattice, forming $Cr_{21}W_2C_6$ [16]. However, higher W-content (alloy Pen. St. 4), cannot go into solution in the carbide lattice and may accommodate in the iron lattice as elemental tungsten causing less strength and deteriorate ductility (strain).

Table 3 presents the mean and standard deviation of Brinell hardness records for the four steels.

Fig. 10 presents mean Brinell hardness values for different steels at the forged state. Little hardness

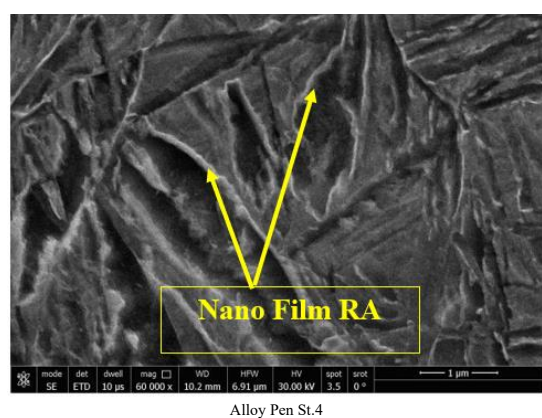
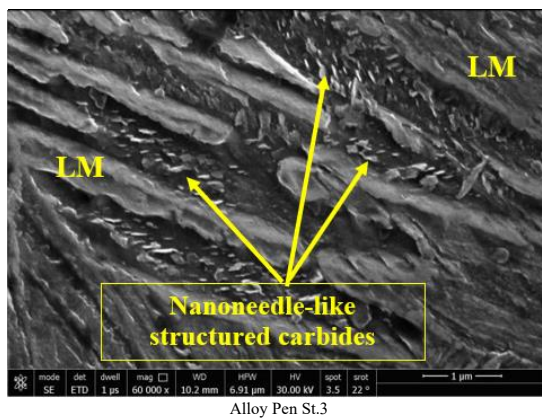
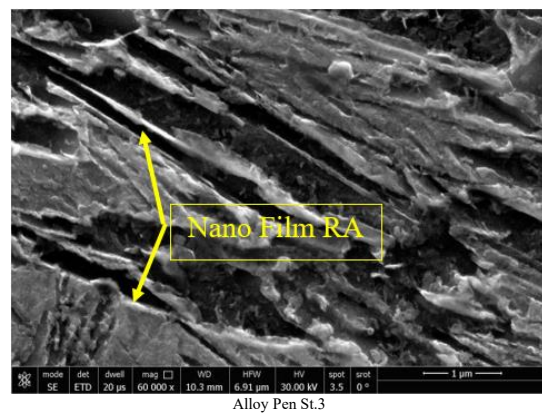
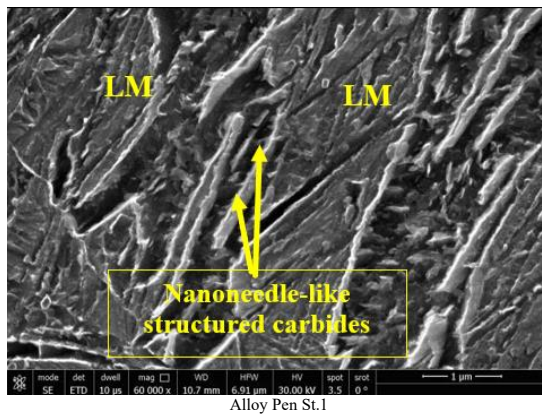


Fig. 7- Nano needle-like structured carbides crammed and located between the fine martensite laths.

Fig. 8- Retained austenite films tightened to the grain boundaries of fine martensite laths.

variation can be observed between 533 and 579 HB, which may be due to uncontrolled of ambient free air cooling after forging. More than 1.6% tungsten content, as in alloy Pen St. 4, has not a pronounced effect on the hardness of the as-forged steels. In a European patent specification No. EP 1 594 997 B1[23], it is stated that the as deformed ultra-high strength steel (Eglin steel) scores at most 48.3 HRC (Hardness Rockwell “C”) which is equivalent to 451 HB, while the present investigation shows a

better score between 533 and 579 HB.

Tempering process usually plays bilateral effects on the steels. The 1st effect concerns with modification of the martensite laths to become coarser, while the 2nd effect is more pronounced on the mechanical properties of the steels. Fig. 11 contains optical microstructure photos after tempering of both steels Pen St 1 and Pen St 4. Both micro-graphs show martensite laths containing speckled carbides spreading all over the martensite matrix (black

Table 3- mean and standard deviation of Brinell hardness records for the four steels

# of steel	Mean value	standard deviation
Pen St. 1	578.82	8.40
Pen St. 2	571.81	6.55
Pen St. 3	533.38	14.17
Pen St. 4	564.28	3.45

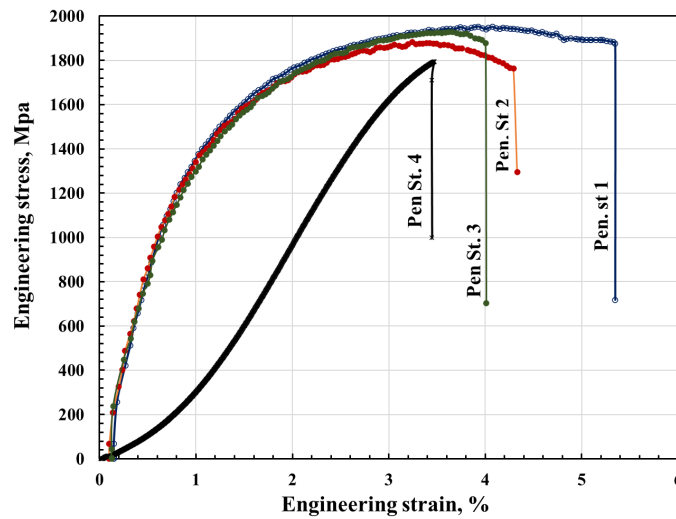


Fig. 9- Engineering stress - Engineering strain relationships.

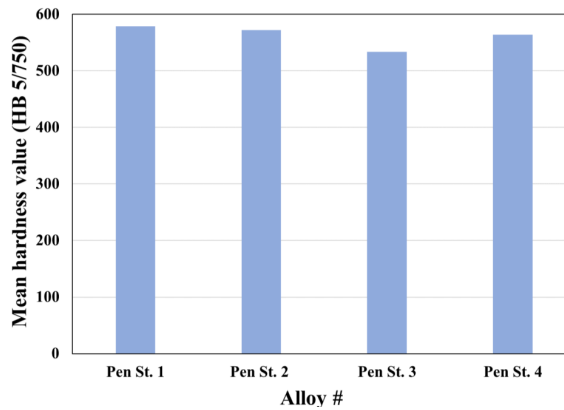


Fig. 10- Mean Brinell hardness values for different steels at the forged state.

points). Tempering process may lead to a degree of freedom for the tempered steels to release and reorganize the crammed needle-like carbides to spread all over the martensite matrix.

Fig. 12 presents microstructure at high magnifications of the tempered steels showing coarsening of the tempered martensite lathes, which is speck-

led with carbides on the surface, while remain of some carbides still exist between the laths.

Furthermore, during tempering, some of the nano needle-like structured carbides, which are crammed between the martensite laths have a chance to migrate out to become free by the effect of the gained tempering temperature [24]. The mi-

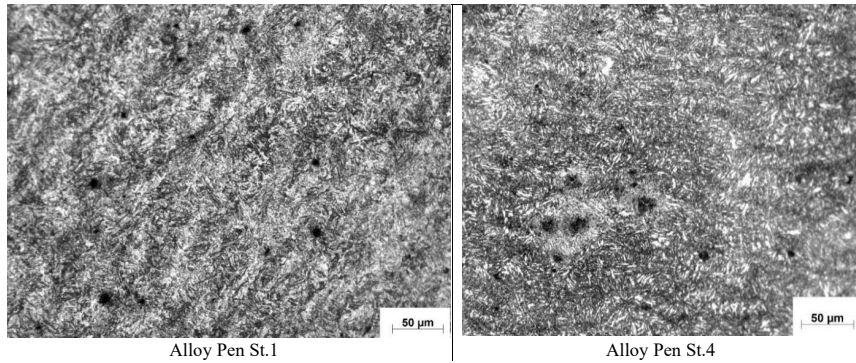


Fig. 11- Optical microstructure photos after tempering of both steels Pen St 1 & Pen St 4.

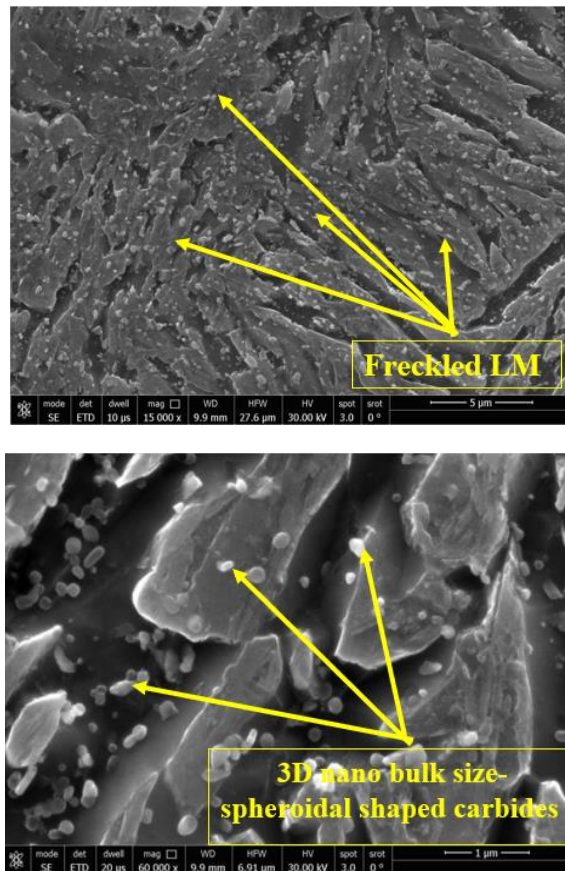


Fig. 12- SEM microstructure presenting coarsening of the tempered martensite lathes speckled with carbides on the surface and remain of some carbides still exist between the laths.

grated nano needle-like carbides favor to coagulate and stick to each other [25] forming 3D nano bulk size- spheroidal shaped carbides sizing 200 nm and precipitating on the martensite laths surface.

Fig. 13 presents SEM Photo and EDX qualitative analysis of speckled carbides, which are spread all over the surface of the tempered martensite laths,

while Fig. 14 presents another SEM Photo and qualitative analysis of the needle like carbides remain between the tempered martensite laths. The analysis of both regions ensures complex carbides formation containing mainly Cr and W beside carbon and many of the minor elements. Available thermodynamic data ensures that Cr-carbides are

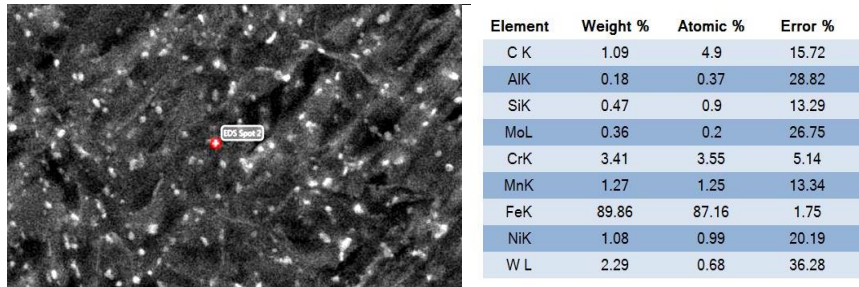


Fig. 13- EDX Photo and qualitative analysis of speckled carbides spread all over the tempered martensite laths.

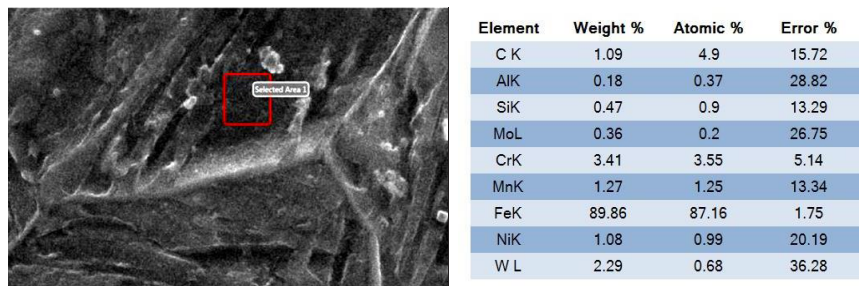


Fig. 14- EDX Photo and qualitative analysis of needle like carbides remain between the tempered martensite laths.

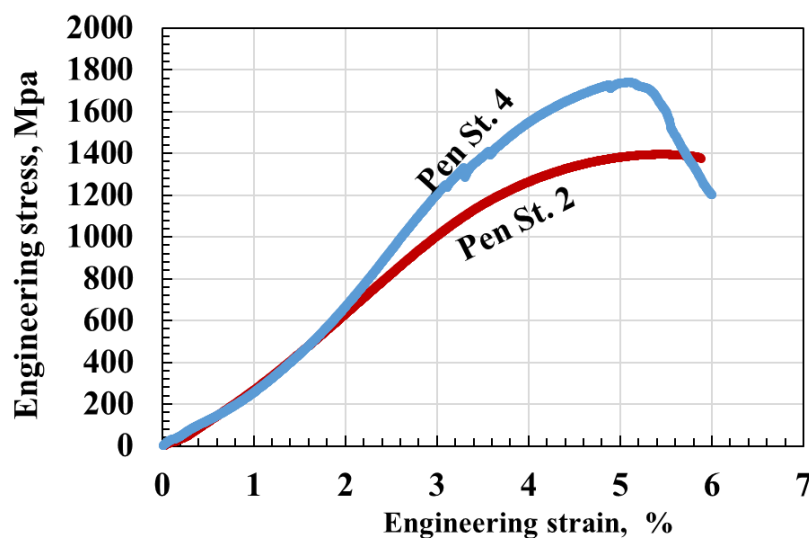


Fig. 15- Engineering stress – engineering strain relationships for steels Pen St2 & Pen St4.

the most stable during the working conditions of steel up to 1400 °C and forming different combinations between carbon and Cr. The most stable carbide is Cr_{23}C_6 with the highest -ve free energy (ΔG°). Mo and W have nearly the same -ve ΔG° , but with lesser value than that for Cr [26, 27]. Due to the chemical composition of the steels under investigation, W has a higher mass action effect. Consequently, the carbides are mostly Cr-W carbides containing minors of Mo. [17].

Mechanical performance of steels after tempering is measured mainly by tensile and Brinell hardness testing. Fig. 15 presents engineering stress – engineering strain relationships for steels Pen St 2 and Pen St4. Both curves possess continuous yielding, where the microstructure is mostly martensite [22,28]. The ultimate strength of Pen St. 2 decreases from 1800 to 1400 MPa after tempering, while the strain increases from 4.3 to 5.9%. Brinell hardness of alloy Pen St. 2 decreases from 580 BH before tempering to about 355.5 BH presenting the same trend effect as in tensile testing.

These changes accompanying tempering are expected and may be attributed to the martensite laths coarsening and due to release of some crammed needle-like carbides and spreading all over the martensite surface as presented previously in Figures 11 and 12. Contrary, no changes in ultimate strength after tempering are noticed on Pen St. 4 and still as 1700 MPa. However, strain increases from 3.4 to 6%. The ultimate strength is not changed may be due to excess of elemental tung-

sten accommodated in the iron lattice of alloy Pen St. 4. The changes in Brinell hardness in alloy Pen St. 4 is very little. It was about 580 HB before tempering and became 563 HB.

Conclusions

1. The XRD charts ensure that the steels possess martensite (M) matrix containing remnant carbides of the alloying elements as $\text{Cr}_{21}\text{W}_2\text{C}_6$ and few amounts of retained austenite phase (RA).

2. Z-parameter calculations expect 0.6 μm grain size after 4-steps directional forging, which is leading to fine martensite laths.

3. SEM detects nano needle-like structured carbides with 50 nm diameter are found crammed and located between the fine martensite laths. Nano films of retained austenite (RA) were found tightening on the boundaries of the -fine lath martensite.

4. A blend of fine martensite laths and nano films of retained austenite (RA) phases in addition to the crammed nano needle-like structured carbides are working cooperatively for ultra-high strength creation.

5. Strength and hardness are increased due to W-addition up to 1.6%, where tungsten may go into solution and accommodate in the carbide lattice, forming $\text{Cr}_{21}\text{W}_2\text{C}_6$.

6. Tempering process may lead to coarsening of the tempered martensite lathes and release to reorganize the crammed needle-like carbides spreading all over the martensite matrix.

References

- O'Loughlin A, Martinez E, Peaslee K, Lekakh S. Effects of Steel Processing on Property Variations in Eglin Steel (ES-1). *Materials Science and Technology*. 2010.
- Xu Z, Ding Z, Dong L, Liang B. Characterization of M_{23}C_6 Carbides Precipitating at Grain Boundaries in 100Mn13 Steel. *Metallurgical and Materials Transactions A*. 2016;47(10):4862-8.
- Leister BM, DuPont JN, Watanabe M, Abrahams RA. Mechanical Properties and Microstructural Evolution of Simulated Heat-Affected Zones in Wrought Eglin Steel. *Metallurgical and Materials Transactions A*. 2015;46(12):5727-46.
- Zhong L, Wang B, Hu C, Zhang J, Yao Y. Hot Deformation Behavior and Dynamic Recrystallization of Ultra High Strength Steel. *Metals*. 2021;11(8):1239.
- El-Bitar T, El-Shenawy E, El-Meligy M, Almosilhy A, Dawood N. Development of Armor High Strength Steel (HSS) Martensitic Plates for Troops Carriers. *Materials Science Forum*. 2016;879:489-94.
- El-Meligy M, El-Bitar T. Hot workability of 420 J1 martensitic stainless steel. *Procedia Manufacturing*. 2020;50:771-6.
- El-Bitar T, El-Meligy M, Khedr M. Roll Pass design, numerical model and processing procedure of a 3rd generation dual phase sheet steel. *Procedia Manufacturing*. 2020;50:173-8.
- Andrew S.P, Caligiuri R.D, Eiselstein L.E. A review of

penetration mechanisms and dynamic properties of tungsten and depleted uranium penetrators. Annual meeting and exhibition of the Minerals, Metals and Materials Society (TMS); 1991 Feb 17-21; New Orleans, LA (US).

9. Ravi Kiran U, Sambasiva Rao A, Sankaranarayana M, Nandy TK. Swaging and heat treatment studies on sintered 90W-6Ni-2Fe-2Co tungsten heavy alloy. *International Journal of Refractory Metals and Hard Materials*. 2012;33:113-21.

10. Luo R, Huang D, Yang M, Tang E, Wang M, He L. Penetrating performance and "self-sharpening" behavior of fine-grained tungsten heavy alloy rod penetrators. *Materials Science and Engineering: A*. 2016;675:262-70.

11. Webb TO, Van Aken DC, Lekakh SN. Evaluating chemical homogeneity in the performance of Eglin steel. *AFS Trans*. 2014 Apr;122:317-33.

12. Jena PK, Mishra B, RameshBabu M, Babu A, Singh AK, SivaKumar K, Bhat TB. Effect of heat treatment on mechanical and ballistic properties of a high strength armour steel. *International Journal of Impact Engineering*. 2010;37(3):242-9.

13. Paules J, Nystrom J, Handerman K. Development and Application of Ultrahigh-Strength Steels for Penetrators. 48th AIAA/ASME/ASCE/AHS/ASC Structures, Structural Dynamics, and Materials Conference; 2007/04/23: American Institute of Aeronautics and Astronautics; 2007.

14. El-Bitar T, ElMeligy M, Borek W, Ebied S. Characterization of Hot Deformation behavior for Ultra-High Strength

- (UHS) Steel containing Tungsten. *Acta Metallurgica Slovaca*. 2023;29(3):144-7.
15. Webb Jr TO. Metallurgical optimization of high strength cast steels with stage I tempering. *Missouri University of Science and Technology*; 2015.
16. Ren F, Chen F, Chen J. Investigation on Dynamic Recrystallization Behavior of Martensitic Stainless Steel. *Advances in Materials Science and Engineering*. 2014;2014:1-16.
17. Thomson RC. Characterization of Carbides in Steels Using Atom Probe Field-Ion Microscopy. *Materials Characterization*. 2000;44(1-2):219-33.
18. Wang L, Speer JG. Quenching and Partitioning Steel Heat Treatment. *Metallography, Microstructure, and Analysis*. 2013;2(4):268-81.
19. Maresca F, Kouznetsova VG, Geers MGD. On the role of interlath retained austenite in the deformation of lath martensite. *Modelling and Simulation in Materials Science and Engineering*. 2014;22(4):045011.
20. Allain SYP, Aoued S, Quintin-Poulon A, Gouné M, Danoix F, Hell J-C, et al. In Situ Investigation of the Iron Carbide Precipitation Process in a Fe-C-Mn-Si Q&P Steel. *Materials (Basel)*. 2018;11(7):1087.
21. Khan W, Tufail M, Chandio AD. Characterization of Microstructure, Phase Composition, and Mechanical Behavior of Ballistic Steels. *Materials (Basel)*. 2022;15(6):2204.
22. ElMeligy M, El-Bitar T. Strain Hardening and Stretch Formability Behavior of Triple Phase (TP) Steel Strips. *Acta Metallurgica Slovaca*. 2021;27(3):152-6.
23. Dilmore M, Ruhlman JD, inventors; Ellwood National Forge Co, assignee. Eglin steel—a low alloy high strength composition. United States patent US 7,537,727. 2009 May 26.
24. Catauro M, Tranquillo E, Dal Poggetto G, Pasquali M, Dell'Era A, Vecchio Cipriotti S. Influence of the Heat Treatment on the Particles Size and on the Crystalline Phase of TiO₂ Synthesized by the Sol-Gel Method. *Materials (Basel)*. 2018;11(12):2364.
25. Sadovnikov SI, Gusev AI. The Effect of Temperature on the Particle Sizes and the Recrystallization of Silver Sulfide Nanopowders. *Physics of the Solid State*. 2018;60(7):1308-15.
26. Anthonysamy S, Ananthasivan K, Kaliappan I, Chandramouli V, Vasudeva Rao PR, Mathews CK, Jacob KT. Gibbs energies of formation of chromium carbides. *Metallurgical and Materials Transactions A*. 1996;27(7):1919-24.
27. Iwai T, Takahashi I, Handa M. Gibbs free energies of formation of molybdenum carbide and tungsten carbide from 1173 to 1573 K. *Metallurgical Transactions A*. 1986;17(11):2031-4.
28. Arribas M, Rana R, Lahaije C, Gómez X, Aranguren I, Pérez I. Design and Properties of 1000 MPa Strength Level Hot-Formed Steels Possessing Dual-Phase and Complex-Phase Microstructures. *Materials Science Forum*. 2018;941:352-7.